

# Double-line terawatt OPCPA laser system for exciting beat wave oscillations

Y. Mori · Y. Kitagawa

Received: 12 July 2012/Revised: 10 October 2012/Published online: 25 November 2012  
© The Author(s) 2012. This article is published with open access at Springerlink.com

**Abstract** A double-line terawatt beat laser (BEAT) is developed for exciting beat wave oscillations. BEAT consists of two oscillators and an amplification system including optical parametric chirped-pulse amplification (OPCPA) in which two individual pulses with wavelength separations of 10–35 nm are amplified, recompressed, and focused as a single beam. The recompressed pulse trace shows that a 150-fs pulse duration full width at half maximum was modulated at a beating period of 72 fs. This beating period matches a resonant excitation of plasma wave with an electron density of  $2.5 \times 10^{18} \text{ cm}^{-3}$ , resulting in excitation of a beat wave in hydrogen plasma with wave amplitude of 15 GV/m. The multiple beating oscillations can amplify the plasma wave and improve its structure. This scheme would be ideal for stabilizing the plasma wave strength in the plasma cavity and for realizing a practical laser plasma accelerator.

## 1 Introduction

Chirped-pulse amplification (CPA) [1] and the self-mode-locked Ti:sapphire laser [2] have revolutionized the production of high-intensity lasers. The electromagnetic field intensities produced by these techniques, which can be greater than  $10^{18} \text{ W/cm}^2$ , yield relativistic electron motion in the laser field [3]. When this relativistic electron motion occurs in a plasma, it creates a wake of plasma oscillation with an electric field strength of gigavolts per meter

through the action of the nonlinear ponderomotive force. That is, a laser-driven plasma accelerator with a higher electric field than that produced by an RF accelerator [4]. For example, the laser plasma accelerators can achieve accelerations of nearly gigaelectronvolts within an acceleration length of only a few centimeters [5–9]. However, a practical laser plasma accelerator requires improved beam stability and repetition.

A stable laser plasma accelerator could be realized by developing (i) an injector, (ii) a plasma accelerating cavity, and (iii) a driving laser. Most laser plasma accelerators apply (i) and (ii) in sequence. For example, a single-pulse laser excites a wakefield, and then electrons are injected from the bulk plasma by self-injection and are accelerated by the nonlinear wake in the bubble regime [10–14]. Such an acceleration scheme uses the strong nonlinear interaction between a high-intensity laser pulse and the plasma. This interaction modulates the laser pulse duration and then disturbs the wave amplitude; therefore, fine control of electron bunches is challenging. This is considered suitable for electron injection or single-stage acceleration because these tasks can be performed independently of the other acceleration components. In contrast, if we applied a staged acceleration with multiple plasma accelerating cavities, we would require a more stable scheme to control both the wave amplitude and the phase among these cavities.

On the other hand, a pulse train from a laser beat wave drives a forced excitation of the plasma wave: beat wave [15, 16]. The pulse duration in the beat wave is determined by the wavelength separation of two-color laser beams, which can be controlled externally rather than within the plasma itself. For example, Umstadter et al. [17] proposed a method for generating large-amplitude wakefield by tailored multiple laser pulses to reduce laser-plasma instabilities. For generating multiple laser pulses, it requires a

Y. Mori (✉) · Y. Kitagawa  
The Graduate School for the Creation of New Photonics  
Industries, 1955-1 Kurematsucho, Nishiku, Hamamatsu,  
Shizuoka 431-1202, Japan  
e-mail: ymori@gpi.ac.jp

high-intensity laser with a two-color spectrum. We developed a double-line Ti:sapphire laser system for a laser particle accelerator that uses the beat wave scheme [18, 19]. This corresponds to the development of (iii), a driving laser, to realize a practical plasma accelerator. Several beat wave lasers have been developed, such as the CO<sub>2</sub> laser [20–22], glass laser [23], and CPA glass laser [24]. They are operated in single-shot mode and are used mainly to reveal the physics of electron laser plasma acceleration. We developed a repetitive beat laser system for plasma particle accelerator applications [26–28].

In this article, we present the double-line ultra-intense CPA system BEAT, focusing on the method by which two individual pulses are amplified, recompressed, and focused as a single beam. To demonstrate the beat wave scheme, a 1.3-TW BEAT laser is applied to excite a wakefield in hydrogen plasma, producing a wake amplitude of 15 GV/m when the electron density matches the resonant density.

## 2 BEAT laser system

The BEAT laser system consists of a laser front end, amplifiers, the rear end and an irradiation chamber. Figure 1 illustrates the layout of BEAT. The front-end and the amplifiers are mounted on a bread board 1.8 × 4.2 m in size. The front end contains two oscillators excited by a single laser-diode-pumped green laser. The seed pulses from those oscillators are co-aligned by a beam splitter (B. S.) into an Öffner stretcher. A pre-amplifier and a power amplifier are used. The pre-amplifier consists of a hybrid system: optical parametric CPA (OPCPA) and a four-pass Ti-sapphire amplifier. The power amplifier is a four-pass Ti-sapphire amplifier. The amplified beam is transferred into a vacuum chamber, where the pulse is compressed by a four-pair grating. The pulse duration is measured using part of the beam consisting of leakage from a dielectric mirror. Another leakage beam is applied as a probe beam to monitor the laser-induced plasma. The compressed beams are fed into the irradiation chamber and focused on the center of the chamber by an off-axial parabolic (OAP) mirror. Several targets can be mounted at the center, such as the gas jet nozzle shown in Fig. 1 and film targets for laser plasma acceleration experiments.

## 3 BEAT front end

Figure 2a shows a diagram of the double-line oscillator used for synchronization, and Fig. 2b shows the double-line spectrum from oscillators with the central wavelengths of  $\lambda_1$  and  $\lambda_2$ , respectively. A single diode-pumped CW laser (Millennia Xs, Spectra Physics) is split into two beams by a

beam splitter to excite two mode-locked Ti:sapphire oscillators (Tsunami-S fs, Spectra Physics), called the master and the slave, respectively. A typical seed pulse has a central wavelength of 800 nm and a full width at half-maximum (FWHM) of 12 nm, and produces a pulse duration of less than 70 fs, an 80 MHz repetition, and a 10 nJ output. We can control the central wavelengths individually between 770 and 830 nm, resulting in double-line spectra with spectral separations of up to 60 nm, as shown in Fig. 2b. The two oscillators are synchronized by a phase-locked loop scheme in which the cavity length of the slave oscillator is controlled by a piezo-electric transducer (PZT) to reduce the phase difference between the pulse frequencies from the master and slave oscillators [29]. Modifying the laser frequency separation by 50 Hz results in a real timing jitter of 3.5 ps.

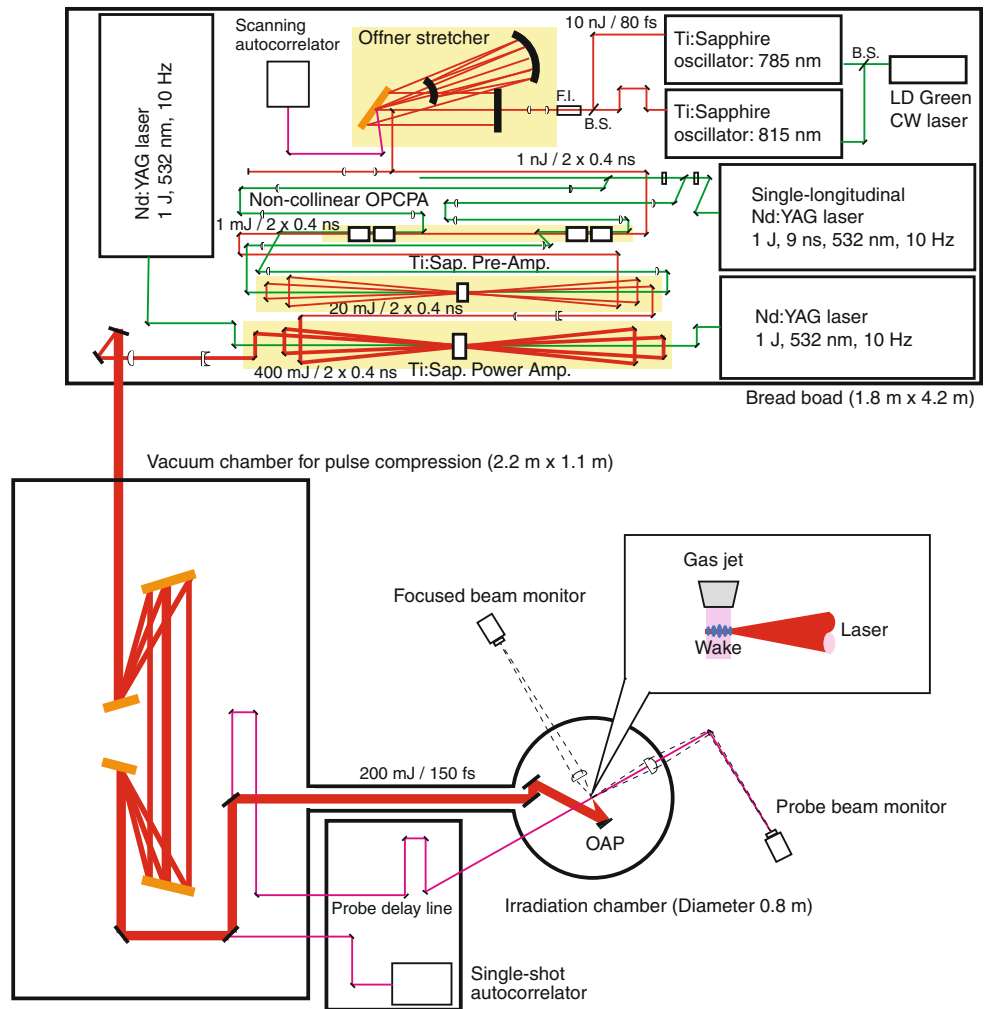
The seed pulses from the oscillators are co-aligned by the beam splitter as a single beam and then sent to a Faraday isolator (F. I.) and a beam expander before entering an aberration-free Öffner-type stretcher [30]. The stretcher is used in a four-pass configuration with a roof mirror and produces a stretching factor of 5,000 for an 80-fs input pulse. It consists of a gold-coated holographic grating with a density of 1,740 lines/mm and a surface flatness of  $\lambda/4$ , a concave mirror (200 mm in diameter) with a 1,000-mm radius of curvature, and a convex mirror (100 mm long, 10 mm height) with a 500-mm radius of curvature. This stretcher is designed for a chirp ratio of 26 ps/nm, and produces an output pulse stretched to 0.4 ns (FWHM) for a single line. The incidence angle is 34.41°, and the diffraction angle is 21.37° relative to the grating surface normal at 800 nm.

## 4 BEAT Amplifiers

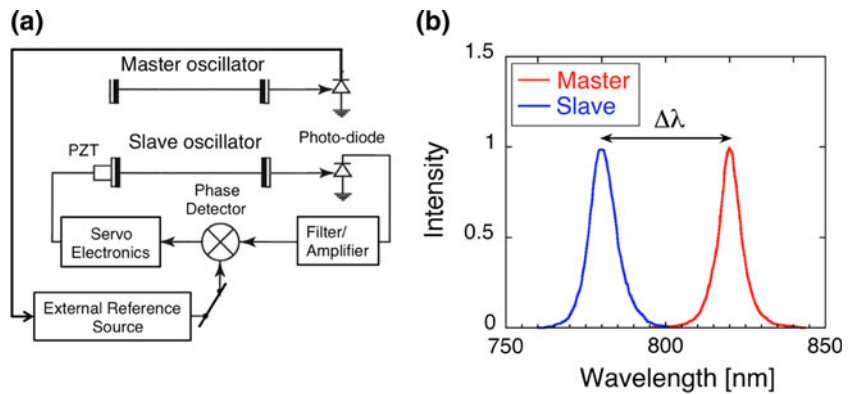
### 4.1 OPCPA

Figure 3a shows the layout for the OPCPA. Two OPCPA stages are arranged in series. The chirped seed pulse from the stretcher has ordinary polarization, and proceeds through the two stages, respectively, experiencing a slight angular change because of its non-parallel incidence against the crystal surface. The pump pulse is provided by a frequency-doubled Nd:YAG laser (Spectra Physics PRO350), which is flash-lamp pumped and generates green pulses of 1,000-mJ with a 10-Hz repetition rate. The pulse longitudinal mode is a single mode produced by an injection seeder with a pulse duration of 9 ns (FWHM). The pump pulse is divided into two beams having extraordinary polarization. We can control each energy by a pair of half-wave-plate (H. W.) and thin-film-polarizer (Pol.) [31].

**Fig. 1** Layout of BEAT laser system, including irradiation chamber



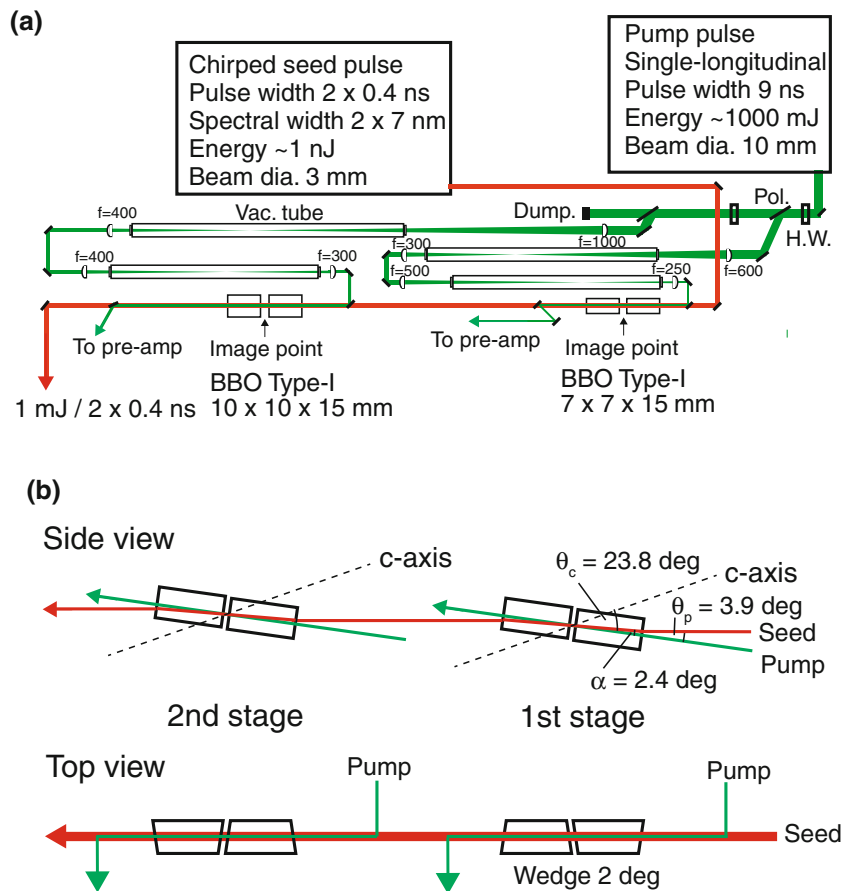
**Fig. 2 a** Diagram of double-line oscillator used for synchronization. **b** Double-line seed spectrum before the stretcher: red ( $\lambda_1$ ) is from the master oscillator, and blue ( $\lambda_2$ ) is from the slave



As shown in Fig. 3b, each stage has two BBO ( $\beta$ -BaB<sub>2</sub>O<sub>4</sub>) crystals of 15-mm in length with cut at 23.8° for type I non-collinear angular phase matching. The first- and second-stage crystals have cross sections of 7 × 7 and 10 × 10 mm<sup>2</sup>, respectively, each with a 2° wedge to eliminate multiple reflections inside the crystals. The

crystals have an inclination of 3.9° with respect to the seed in order to satisfy non-collinear angular phase matching of 2.4° inside the crystal. The pump injection angle is normal to the crystal surface. In this configuration, the theoretical gain bandwidth for a single pass is >300 nm (FWHM) with 5-mm thick crystals [32]. With 15-mm thick crystals, the

**Fig. 3 a** Schematic layout of the OPCPA system. **b** Non-collinear BBO layout



measured bandwidth of amplified optical parametric fluorescence (AOPF) was 180 nm, which satisfies our required bandwidth of 60 nm. An image of the output pulse, where 1 m far from a KDP crystal in the YAG laser head, is relayed into the center of the BBO crystals in each stage. At the center, the seed diameter ( $1/e^2$ ) is 3 mm, and the pump diameter ( $1/e^2$ ) is 2.5 mm for the first stage and 4 mm for the second stage.

Figure 4a shows the seed energy gain as a function of the pump intensity for the first stage with an input seed energy of 1 nJ and for the second stage with energies of 1.6 and 9.8  $\mu\text{J}$ . For a small seed energy input, the gain increases exponentially as the pump intensity increases. At the first stage, a maximum gain of  $3 \times 10^5$  was achieved with a pump intensity of 500  $\text{MW}/\text{cm}^2$  for the seed energy of 1 nJ. At the second stage, when the seed energy is high, the gain curve indicates saturation as the pump intensity increases. Figure 4b shows the output energy from the second-stage OPCPA as a function of the input pump energy. We achieved an energy of 2.5 mJ at a pump energy of 300 mJ and input energy of 9.8  $\mu\text{J}$ . However, in this case, the amplified optical parametric fluorescence (AOPF) contained 0.7 mJ: 30 % of the total energy. We confirmed this by blocking the seed pulse at the oscillators. When this

pulse goes through a power amplifier, the AOPF increases the foot pulse which decreases the peak intensity. To suppress the AOPF, we operated the second stage at an input energy of 1.6  $\mu\text{J}$  and a pump energy of less than 300 mJ, producing an output energy of 1 mJ.

Figure 5a shows the temporal pulse train of OPCPA. The two peaks indicate the amplified double-line spectra. We can control the double-line peaks by tuning the angle of the BBO crystal for each stage [33]. In OPCPA, changing

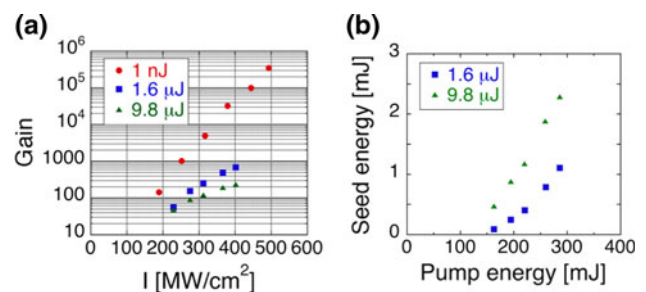


**Fig. 4 a** OPCPA energy gain as a function of pump intensity in two-stage BBO crystal layout. Solid-circles, rectangles, and triangles represent seed energies of 1 nJ in first stage, 1.6  $\mu\text{J}$  in second stage, and 9.8  $\mu\text{J}$  in second stage, respectively. **b** Output energy from the second-stage OPCPA as a function of input pump energy

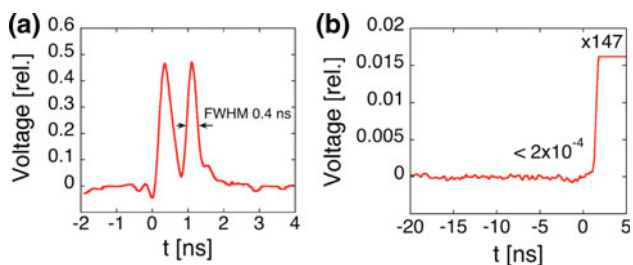


Fig. 5 a OPCPA pulse train. b Pedestal ratio of OPCPA pulse

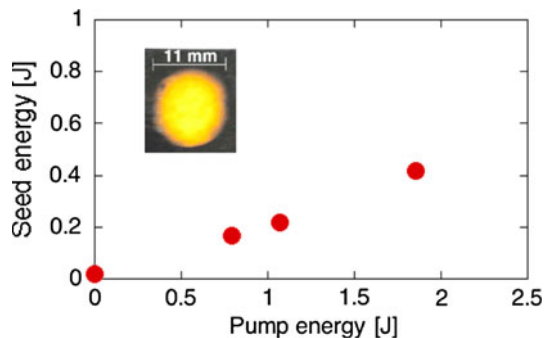


Fig. 6 Energy extracted from the power amplifier. Insert: amplified beam burn pattern

of the phase-matching condition makes it possible to tune the central wavelength of the amplified pulse. Therefore, rough spectral shaping of the amplified pulse in a given spectral range can be achieved by cascading two BBO crystals working under slightly different phase matching conditions. Figure 5b shows the temporal contrast of the amplified pulse. The measured pedestal contrast before compression was  $2 \times 10^{-4}$ , therefore, it is estimated to be less than  $10^{-7}$  after recompression.

#### 4.2 Multi-pass Ti:sapphire amplifications

After the OPCPA system, there are two multi-pass Ti:sapphire amplifier stages. The first stage is a four-pass pre-amplifier, which consists of a Ti:sapphire crystal 10 mm long and 15 mm in diameter that is pumped by the

remaining pump beam after the OPCPA. The image of the pump beam near the BBO crystals is relayed again in air on the surface of the Ti:sapphire crystal. The seed pulse into this pre-amplifier is expanded to 4 mm ( $1/e^2$ ) by a pair of convex and concave lenses. The output seed energy was 20 mJ. In combination with OPCPA, this pre-amplifier is pumped by a single laser, enabling a hybrid amplifier system [34].

The second stage is also a four-pass power amplifier, which consists of a Ti:sapphire crystal 10 mm long and 20 mm in diameter with an anti-refractive coating. This crystal is pumped by two frequency-doubled Nd:YAG lasers each laser provides pulses directly to one side. The beam diameter ( $1/e^2$ ) is 11 mm. The input seed pulse is expanded to 12 mm ( $1/e^2$ ) by a pair of convex and concave lenses. This pulse was amplified to 420 mJ, as shown in Fig. 6. The crystal has an absorption efficiency of the seed laser with 0.15 for one pass. This limits an extraction efficiency relatively low as 0.23. The amplified beam diameter was estimated to be 11 mm from a beam burn pattern on Polaroid film.

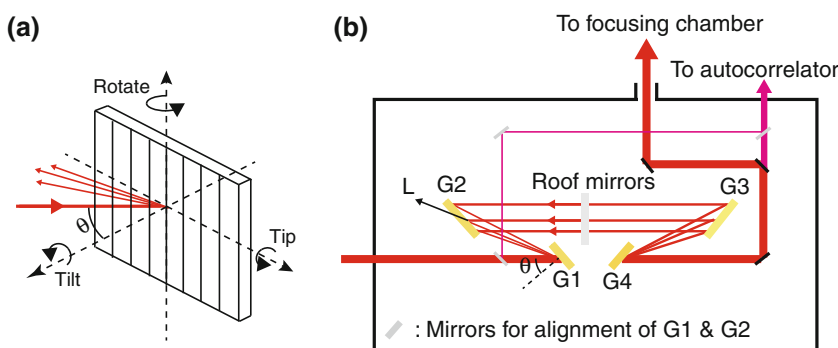
### 5 Rear end

#### 5.1 Pulse compression

After these amplifier stages, the beam is expanded to 35 mm ( $1/e^2$ ) by a pair of concave and convex lenses. This expanded beam is sent from the breadboard into a vacuum pulse chamber that is 2.2 m long and 1.1 m wide [ Fig. 1]. Figure 7a, b shows the geometry of the grating alignment axis and a schematics of the pulse compression grating, respectively. The latter consists of four gold-coated gratings (G1,G2,G3, and G4) with a grooving density of 1740 g/mm and a cross section of  $210 \times 70 \text{ mm}^2$ . After pulse compression, the pulse leakage from the dielectric mirror is sent into a probe system in which autocorrelation pulse duration measurements are performed.

To finally recompress the double-line pulses, we first placed a roof mirror as shown in Fig 7b to align gratings

Fig. 7 a Geometry of the grating alignment axis. b Configuration of the pulse compression gratings



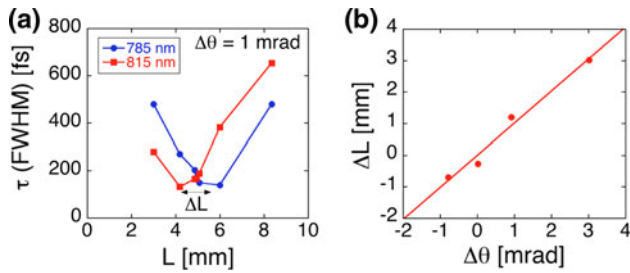


**Fig. 8** **a** Recompressed amplified pulse duration (FWHM) as a function of grating distance  $L$  (relative value). **b** Grating distance differences  $\Delta L$  as a function of grating incident angle differences  $\Delta\theta$ .

G1 and G2. The gratings are aligned by changing the grating incident angle  $\theta$  and grating distance  $L$  (relative value) to minimize an optimized pulse duration differences between the two pulses. The grating angle of G2 is also changed so that the two gratings have the same angle. The pulse duration is measured by a single-shot autocorrelator (Reef-SS, Delmar Photonics). Figure 8a shows the duration of the recompressed pulses (FWHM) as a function of  $L$  at  $\Delta\theta = 1$  mrad, which is the grating incident angle from the optimization. To obtain the pulse duration of a single line, we cut a seed pulse from another oscillator in the front end. Each pulse had an optimized pulse duration at each  $L$ , a difference in  $L$  ( $\Delta L$ ) indicates a mismatch in the grating incident angle for optimized double-line recompression. For example, at  $\Delta\theta = 1$  mrad, a 785-nm beam has a 150 fs duration at  $L = 6$  mm, and an 815-nm beam has a duration of 150 fs at  $L = 4$  mm. Figure 8b shows the optimized grating distance differences  $\Delta L$  as a function of the differences in the grating incident angle  $\Delta\theta$ . The optimized grating incident angle ( $\Delta\theta = 0$ ) is achieved when  $\Delta L$  reaches zero. After gratings G1 and G2 were aligned, we aligned gratings G3 and G4 using the same algorithm. The total diffraction efficiency of the four gratings was 50%.

Figure 9a shows an image of the recompressed amplified double-line pulse second-order autocorrelation image (upper) and its temporal trace, and Fig. 9b shows the amplified double-line spectrum. We obtained beating in the

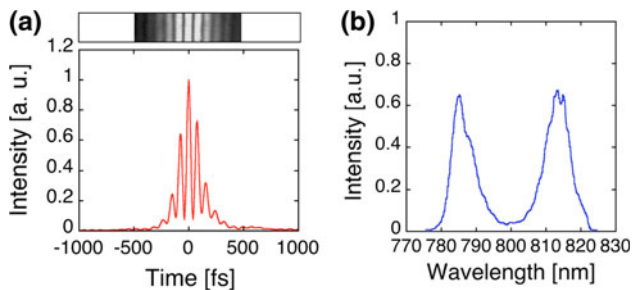


**Fig. 9** **a** Recompressed amplified double-line pulse second-order auto correlation: image (upper) and its temporal trace. **b** Amplified double-line spectrum

recompressed pulse when the double-line laser was synchronized in time, the second-order autocorrelation image shows that the 150-fs pulse (FWHM) was modulated at a beat period  $\tau_{\text{beat}}$  of 72 fs.

## 5.2 Beam focusing

The recompressed pulse is sent into the focusing chamber, which contains a 2" diameter gold-coated OAP mirror with a focal length of 138 mm ( $f/3.9$ ). The beam spot is measured by a beam monitor consisting of a convex lens and a CCD camera that provides  $27\times$  magnification. Figure 10a, b shows the beam focusing profile of the double-line pulse without optimization, with optimization of the G4 grating's tilt and rotation angles, and optimization of the OAP mirror's tilt and rotation angles. Without optimization of the G4 angles, the beam profile has two spots caused by spatial chirping, which indicates that the double pulse does not overlap in space. Their vertical and horizontal separations can be minimized by tuning the G4 tilt and rotation configuration, respectively. In addition, after optimization of the OAP mirror tilt and rotation angles, the optimized spot size is  $7.7 \times 9 \mu\text{m}^2$  FWHM. In  $1/e^2$  of the beam spot, 32 % of the total energy is contained. The recompressed double-line pulse has an energy of 200 mJ and a pulse duration (FWHM) of 150 fs: the resulting peak power and focal intensity are 1.3 TW and  $7.8 \times 10^{17} \text{ W/cm}^2$ , respectively.

## 6 Beat wave excitation by BEAT

To demonstrate resonant plasma wave excitation, we focused this double-line laser pulse on a supersonic hydrogen gas jet flow situated at the center of the focusing chamber, as shown in Fig. 1. The spectral separation  $\Delta\lambda$  was 30 nm, and the corresponding resonant electron density was  $2.5 \times 10^{18} \text{ cm}^{-3}$ . The plasma-wave excitation was confirmed by the scattered laser light in the higher-harmonic sidebands, detected with a spectrometer. The wave amplitude was evaluated from these normalized sideband intensities. The electron density varied linearly

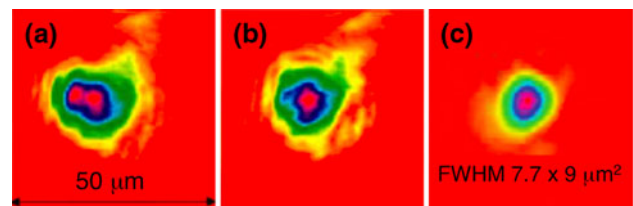


**Fig. 10** Beam focusing profile of double-line pulses: **a** before optimization, **b** after optimization of G4 grating tilt and rotation, and **c** after optimization of the OAP mirror tilt and rotation

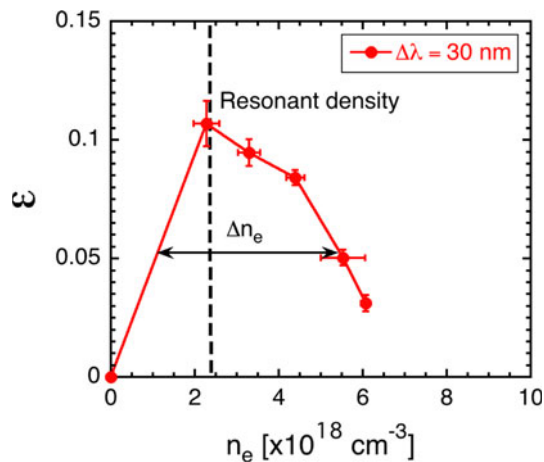


**Fig. 11** Amplitude of the density fluctuations  $\epsilon$  as a function of electron density  $n_e$  for  $\Delta\lambda = 30$  nm. Dashed line represents theoretically resonant density. Arrow represents the resonant electron density width  $\Delta n_e$  (FWHM)

with the backing pressure from the vacuum. Therefore, a variation of a normalized sideband intensities versus backing gas jet pressure reveals a resonant conditions. The details of the experimental setup and detailed results are given in Ref. 19. Figure 11 shows the amplitude of the density fluctuation  $\epsilon = \delta n_e/n_e$  as a function of the electron density  $n_e$ . A peak value of  $\epsilon$  appears at the theoretically predicted resonant density (dashed line) indicating successful beat wave excitation. The resonant electron density width  $\Delta n_e$  (FWHM) is  $4.5 \times 10^{18} \text{ cm}^{-3}$ . According to plasma acceleration theory, the electric field of the plasma wave is given by  $96\epsilon\sqrt{n_e}[10^{18}\text{cm}^{-3}] \text{ GV/m}$  [16]; therefore, at the resonant density,  $\epsilon = 0.1$  corresponds to 15 GV/m. This result suggests that, if we succeed in extending the laser propagating length to around 10 cm by using a capillary plasma [5, 6, 7, 8, 35, 36], we can achieve a GeV-class accelerating cavity with a 10-cm length.

We also demonstrated the control of the beat bunch duration, this is, the duration at which laser pulse are modulated by the beat laser by tuning the spectral separation of the double-line oscillators  $\Delta\lambda$ ; the results are shown in Fig. 12a. The solid curve represents the theoretical duration, which is given by  $\tau_{beat} = \lambda_1\lambda_2/(c\Delta\lambda)$ , where  $c$  is the speed of light. We successfully controlled  $\tau_{beat}$  within a  $\Delta\lambda$  range of from 10 to 35 nm. These experimental values agree well with the theory. The grating size limits  $\Delta\lambda > 35$  nm operation, because the width of the diffracted laser pulse is wider than the grating size. Figure 12b shows the resonant electron density as a function of  $\Delta\lambda$ . The solid circle represents experimental data from Fig. 11, and the solid curve is based on theory. The error bar represents the resonant electron density width  $\Delta n_e$  shown in Fig. 11.

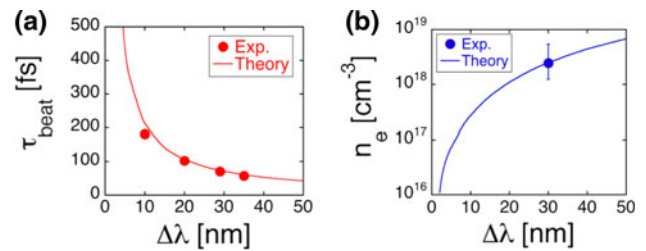


**Fig. 12** **a** Beat bunch duration  $\tau_{beat}$  as a function of double-line spectral separation  $\Delta\lambda$ : solid circles and solid curve represent experimental and theoretical data, respectively. **b** Resonant electron density as a function of  $\Delta\lambda$ : solid circles and solid curve represent experimental data (from Fig. 11) and theoretical calculation, respectively

When we apply the linear wakefield acceleration theory [16], the maximum accelerating energy gain is given by  $1.7\epsilon/n_e[10^{18}\text{cm}^{-3}] \text{ GeV}$ . The control range of  $\Delta\lambda$  we obtained enables beat wave at electron densities between  $3 \times 10^{18}$  to  $3 \times 10^{17} \text{ cm}^{-3}$ , for a maximum gain control between  $0.56\epsilon$  and  $5.6\epsilon \text{ GeV}$ . This plasma wave excitation scheme would be ideal for stabilizing the plasma wave strength in the plasma cavity in combination with an injector and multiple of plasma wake cavity stages.

### 7 Conclusions

To demonstrate beat-wave laser plasma acceleration, we developed the double-line ultra-intense CPA system BEAT. It includes two oscillators and a hybrid system via OPCPA and Ti:sapphire multi-pass amplifiers and provides a double-line spectrum with a spectral separation of 10–35 nm. The OPCPA pre-amplifier provides individual tuning of the amplitude of each line in the double-line spectrum, resulting in a pedestal ratio of  $10^{-7}$  after pulse recompression. Two stages of multipass Ti:sapphire amplification provide a 200-mJ output after recompression. The two individual pulses can be recompressed and focused to act like a single beam by aligning the grating angles. The compressed pulse trace shows multiple laser-beating bunches of 72 fs within a pulse duration of 150 fs, which is consistent with the theoretically predicted behavior.

In addition, we apply the BEAT system, which has a peak power of 1.3 TW and focal intensity of  $7.8 \times 10^{17} \text{ W/cm}^2$ , to beat wave excitation in hydrogen plasma. The resulting wave amplitude was 15 GV/m when the electron density matched the resonant density. We also succeeded in double-line amplification with a spectral separation of 10–35 nm, yielding resonant electron density control over a range of one order of magnitude (from  $3 \times 10^{17}$  to  $3 \times 10^{18} \text{ cm}^{-3}$ ).

**Acknowledgments** This work was supported by the Advanced Compact Accelerator Development Project of the Ministry of Education, Culture, Sports, Science and Technology and the National Institute of Radiological Sciences, Japan. The authors thank Y. Sakawa, ILE, Osaka University for the ILE-GPI collaboration research #B2-4I; K. Kondo, JAEA; and S. Nakai, GPI.

**Open Access** This article is distributed under the terms of the Creative Commons Attribution License which permits any use, distribution, and reproduction in any medium, provided the original author(s) and the source are credited.

## References

1. D. Strickland, G. Mourou, *Opt. Commun.* **56**, 219 (1985)
2. D.E. Spence, P.N. Kean, W. Sibbett, *Opt. Lett.* **16**, 42 (1991)
3. G.A. Mourou, T. Tajima, S.V. Bulanov, *Rev. Mod. Phys.* **78**, 309 (2006)
4. T. Tajima, J.M. Dawson, *Phys. Rev. Lett.* **43**, 207 (1979)
5. W.P. Leemans, B. Nagler, A.J. Gonsalves, C.s. Tóth, K. Nakamura, C.G.R. Geddes, E. Esarey, C.B. Schroeder, S.M. Hooker, *Nature Phys.* **2**, 690 (2006)
6. K. Nakamura, B. Nagler, Cs. Tóth, C.G.R. Geddes, C.B. Schroeder, E. Esarey, A.J. Gonsalves, S.M. Hooker, W.P. Leemans, *Phys. Plasmas* **14**, 056708 (2007)
7. T. Kameshima, W. Hong, K. Sugiyama, X. Wen, Y. Wu, C. Tang, Q. Zhu, Y. Gu, B. Zhang, H. Peng, S. Kurokawa, L. Chen, T. Tajima, T. Kumita, K. Nakajima, *Appl. Physics Express* **1**, 066001 (2008)
8. T. Kameshima, H. Kotaki, M. Kando, I. Daito, K. Kawase, Y. Fukuda, L.M. Chen, T. Homma, S. Kondo, T.Z.h. Esirkepov, N.A. Bobrova, P.V. Sasorov, S.V. Bulanov, *Phys. Plasmas* **16**, 093101 (2009)
9. C.E. Clayton, J.E. Ralph, F. Albert, R.A. Fonseca, S.H. Glenzer, C. Joshi, W. Lu, K.A. Marsh, S.F. Martins, W.B. Mori, A. Pak, F.S. Tsung, B.B. Pollock, J.S. Ross, L.O. Silva, D.H. Froula, *Phys. Rev. Lett.* **105**, 105003 (2010)
10. S.P.D. Mangles, C.D. Murphy, Z. Najmudin, A.G.R. Thomas, J.L. Collier, A.E. Dangor, E.J. Divall, P.S. Foster, J.G. Gallacher, C.J. Hooker, D.A. Jaroszynski, A.J. Langley, W.B. Mori, P.A. Norreys, F.S. Tsung, R. Viskup, B.R. Walton, K. Krushelnick, *Nature* **431**, 535 (2004)
11. C.G.R. Geddes, Cs. Toth, van J. Tilborg, E.H. Esarey, C.B. Schroeder, D. Bruhwiler, C. Nieter, J. Cary, W.P. Leemans, *Nature* **431**, 538 (2004)
12. J. Faure, Y. Glinec, A. Pukhov, S. Kiselev, S. Gordienko, E. Lefebvre, J.-P. Rousseau, F. Burgy, V. Malka, *Nature* **431**, 541 (2004)
13. E. Miura, K. Koyama, S. Kato, N. Saito, M. Adachi, Y. Kawada, T. Nakamura, M. Tanimoto, *Appl. Phys. Lett.* **86**, 251501 (2005)
14. A. Pukov, Meyer-ter- Vehn: *J. Appl. Phys. B* **74**, 355 (2002)
15. T. Tajima, *Laser Part. Beams* **3**, 351 (1985)
16. N.A. Ebrahim, S.R. Douglas, *Laser Part. Beams* **13**, 147 (1995)
17. D. Umstadter, E. Esarey, Kim *J Phys. Rev. Lett.* **72**, 1224 (1994)
18. Y. Mori, S. Fukumochi, Y. Hama, K. Kondo, Y. Sentoku, Y. Kitagawa, *Int. J. Mod. Phys. B* **21**, 572 (2007)
19. Y. Mori, Y. Kitagawa, *Phys. Plasmas* **19**, 053106 (2012)
20. Y. Kitagawa, T. Matsumoto, T. Minamihata, K. Sawai, K. Matsuo, K. Mima, K. Nishihara, H. Azechi, K.A. Tanaka, H. Takabe, S. Nakai, *Phys. Rev. Lett.* **68**, 48 (1992)
21. C.E. Clayton, K.A. Marsh, A. Dyson, M. Everett, A. Lai, W.P. Leemans, R. Williams, Joshi *C Phys. Rev. Lett.* **70**, 37 (1993)
22. S.Ya Tochitsky, R. Narang, C.V. Filip, P. Musumeci, C.E. Clayton, R.B. Yoder, K.A. Marsh, J.B. Rosenzweig, C. Pellegrini, C. Joshi, *Phys. Rev. Lett.* **92**, 095004 (2004)
23. F. Amiranoff, M. Laberge, J.R. Marques, F. Moulin, E. Fabre, B. Cros, G. Matthieussent, P. Benkheiri, F. Jacquet, J. Meyere, P. Mine, C. Stenz, P. Mora, *Phys. Rev. Lett.* **68**, 3710 (1992)
24. B. Walton, Z. Najmudin, M.S. Wei, C. Marle, R.J. Kingham, K. Krushelnick, A.E. Dangor, R.J. Clarke, M.J. Poulter, C. Hernandez-Gomez, S. Hawkes, D. Neely, J.L. Collier, C.N. Danson, *Opt. Lett.* **27**, 2203 (2002)
25. B. Walton, Z. Najmudin, M.S. Wei, C. Marle, R.J. Kingham, K. Krushelnick, A.E. Dangor, R.J. Clarke, M.J. Poulter, C. Hernandez-Gomez, S. Hawkes, D. Neely, J.L. Collier, C.N. Danson, S. Fritzler, V. Maika, *Phys. Plasmas*, 13013103 (2006)
26. H. Kuwabara, Y. Mori, Y. Kitagawa, *Plasma Fusion Res.* **3**, 003 (2008)
27. S. Ootsuka, Y. Mori, T. Makino, M. Ohta, H. Kuwabara, Y. Kitagawa, *Rev. Laser Eng.* **38**, 386 (2010)
28. Y. Mori, H. Kuwabara, K. Ishii, R. Hanayama, T. Kawashima, Y. Kitagawa, *Appl. Phys. Express* **5**, 056401 (2012)
29. *Tsunami user's manual (Spectra Physics, 2002)*
30. G. Cheriaux, P. Rousseau, F. Salin, J.P. Chambaret, W. Barry, L.F. Dimauro, *Opt. Lett.* **21**, 414 (1996)
31. H. Yoshida, E. Ishii, R. Kodama, H. Fujita, Y. Kitagawa, Y. Izawa, T. Yamanaka, *Opt. Lett.* **28**, 257 (2003)
32. N. Ishii, L. Turi, V.S. Yakovlev, T. Fuji, F. Krausz, A. Baltuska, R. Butkus, G. Veitas, V. Smilgevicius, R. Danielius, A. Piskarskas, *Opt. Letters* **30**, 567 (2005)
33. H. Kiriya, N. Inoue, Y. Akahane, K. Yamakawa, *Opt. Express* **14**, 438 (2006)
34. I. Jovanovic, C.A. Ebberts, C.P.J. Barty, *Opt. Lett.* **27**, 1622 (2002)
35. Y. Kitagawa, Y. Sentoku, S. Akamatsu, W. Sakamoto, R. Kodama, K.A. Tanaka, K. Azumi, T. Norimatsu, T. Matuoka, H. Fujita, H. Yoshida, *Phys. Rev. Lett.* **92**, 205002 (2004)
36. Y. Mori, Y. Sentoku, K. Kondo, K. Tsuji, N. Nakanii, S. Fukumochi, M. Kashihara, K. Kimura, K. Takeda, K.A. Tanaka, T. Norimatsu, T. Tanimoto, H. Nakamura, M. Tampo, R. Kodama, E. Miura, K. Mima, Y. Kitagawa, *Phys. Plasmas* **16**, 123103 (2009)